Broadband Analysis Including Beam Steering of Phased Array Antennas by Order Reduction

O. Floch, A. Sommer, O. Farle, and R. Dyczij-Edlinger
Chair for Electromagnetic Theory, Saarland University, Saarbrücken D-66123, Germany

Abstract— This paper combines projection-based model-order reduction and the empirical interpolation method to generate an efficient numerical procedure for analyzing electrically large antenna arrays at the fields level. The method handles arbitrary aperture illuminations over wide frequency bands and yields both circuit parameters and farfield patterns. A numerical example demonstrates the benefits of the suggested approach.

1. INTRODUCTION

Phased antenna arrays are capable of producing a variety of beam forms over a wide range of scan angles, over wide frequency bands. Ideally, their farfield patterns are obtained as the product of element and array factors. In practice, however, parasitic coupling of antenna elements causes deviations in the farfield patterns, or even to scan blindness. Moreover, resonant radiators get detuned, and input impedances vary across the array.

Numerical fields simulation methods, such as the finite-element (FE) method, include such parasitic effects but tend to be very time-consuming: The large electric size and number of radiators of typical antenna arrays lead to FE matrices of large dimension and large numbers of right-hand sides (RHS). When iterative solvers are employed, the availability of efficient preconditioners is of utmost importance. For electrically large structures, domain decomposition (DD) methods have proven to be highly effective. Still, solving the large-scale FE system remains expensive, particularly when broad frequency bands are to be covered.

To reduce computational efforts, we propose a two-step model order reduction (MOR) approach similarly to [1, 2], but with the focus on electrically large structures: We first construct a reduced-order model (ROM) for the frequency-dependent nearfields and circuit parameters. For this purpose, a multi-point MOR method with self-adaptive expansion point selection [3] is employed. The second step utilizes the empirical interpolation method (EIM) [4] to construct an affine approximation to the nearfield to farfield (NF-FF) operator as a function of frequency f and look angles (θ, ϕ). The resulting model has a small memory footprint, and typical ROM solution times are fractions of a second on a low-cost PC. The proposed method does not only produce circuit parameters (S matrices) but also farfield patterns for arbitrary excitations. It is therefore well-suited for advanced applications such as broadband antenna pattern synthesis. A numerical example is presented to demonstrate the characteristic features of the suggested approach.

2. TIME-HARMONIC BOUNDARY VALUE PROBLEM

In the following, a bounded domain $\Omega \subset \mathbb{R}^3$ with boundary $\partial\Omega$ and outward-unit normal $\hat{\mathbf{n}}$ is considered. The boundary consists of electric walls Γ_E, absorbing boundaries Γ_{ABC}, and T ports $\Gamma_{P_1}, \ldots, \Gamma_{P_T}$. The electric field is denoted by $\mathbf{E}$, the magnetic field by $\mathbf{H}$, the relative magnetic permeability by μ_r, the relative electric permittivity by ϵ_r, and the electric conductivity by σ. The abbreviations k_0 and η_0 stand for the free-space wave number and characteristic impedance, respectively. The excitation of port m is given by the surface current density $\mathbf{K}^m$.

We consider the time-harmonic boundary value problem (BVP)

$$\nabla \times \mu_r^{-1} \nabla \times \mathbf{E} + jk_0\eta_0\sigma\mathbf{E} - k_0^2\epsilon_r\mathbf{E} = \mathbf{0} \qquad \text{in } \Omega, \tag{1a}$$

$$\pi_t(\mathbf{E}) = \mathbf{0} \qquad \text{on } \Gamma_E, \tag{1b}$$

$$\left[\mu_r^{-1}\nabla \times \mathbf{E}\right] = -jk_0\eta_0\mathbf{K}^m \qquad \text{on } \Gamma_{P_m}, \tag{1c}$$

$$\gamma_t\left(\mu_r^{-1}\nabla \times \mathbf{E}\right) - jk_0\sqrt{\tfrac{\epsilon_r}{\mu_r}}\pi_t(\mathbf{E}) = \mathbf{0} \qquad \text{on } \Gamma_{ABC}. \tag{1d}$$

Here, $\gamma_t(\mathbf{E}) := \hat{\mathbf{n}} \times \mathbf{E}$ denotes the tangential trace and $\pi_t(\mathbf{E}) := \hat{\mathbf{n}} \times (\mathbf{E} \times \hat{\mathbf{n}})$ the tangential component trace mapping [5]. The jump operator $[\mathbf{E}]$ is defined by $[\mathbf{E}] : [\mathbf{E}]_{ij} := \gamma_t(\mathbf{E}_i) + \gamma_t(\mathbf{E}_j)$.

3. NUMERICAL APPROXIMATION OF THE BOUNDARY VALUE PROBLEM

Discretizing the BVP (1) by a FE-DD method results in an affinely parametrized linear system of equations [6, 7] of the general form

$$\left(\sum_{i=1}^{I} f_i(k_0)\mathbf{A}_i\right)\mathbf{X}(k_0) = g(k_0)\mathbf{B}, \tag{2}$$

where $\mathbf{X} \in \mathbb{C}^{N\times T}$ denotes the solution matrix. Both the functions $f_i(k_0) : \mathbb{R} \to \mathbb{C}$ and $g(k_0) : \mathbb{R} \to \mathbb{C}$ and the matrices $\mathbf{A}_i \in \mathbb{C}^{N\times N}$ and $\mathbf{B} \in \mathbb{C}^{N\times T}$ are independent of the wavenumber. The matrix $\mathbf{B}$ contains excitation vectors $\mathbf{b}_m$ according to single port excitations, i.e.,

$$\mathbf{B} = [\mathbf{b}_1\mathbf{b}_2 \ldots \mathbf{b}_T] \in \mathbb{C}^{N\times T}. \tag{3}$$

4. MODEL ORDER REDUCTION

Since the block FE-DD system (2) exhibits affine wavenumber-dependence, it is well-suited for projection-based MOR [3]. Let $\mathbf{x}_m(k_0) \in \mathbb{C}^N$ be the solution of the linear system

$$\left(\sum_{i=1}^{I} f_i(k_0)\mathbf{A}_i\right)\mathbf{x}_m(k_0) \quad = g(k_0)\mathbf{b}_m. \tag{4}$$

A multi-point ROM is built from the FE solutions $\mathbf{x}_m(k_0^i)$ of (4) at M expansion points $k_0^1, \ldots, k_0^M$, with $M \ll N$. The expansion points k_0^i as well as the excitation vector $\mathbf{b}_m$, for which (4) is solved, are selected adaptively; see Section 4.1. Next, a unitary projection matrix $\mathbf{V} \in \mathbb{C}^{N\times M}$ is computed such that

$$\mathbf{X} \quad \approx \mathbf{V}\tilde{\mathbf{X}} \quad \text{with range}\,(\mathbf{V}) = \text{span}\left\{\mathbf{x}(k_0^i)\right\}, \quad i = 1\ldots M. \tag{5}$$

Then, Galerkin projection leads to a ROM of the form

$$\left(\sum_{i=1}^{I} f_i(k_0)\tilde{\mathbf{A}}_i\right)\tilde{\mathbf{X}}(k_0) \quad = g(k_0)\tilde{\mathbf{B}}, \tag{6}$$

wherein the reduced matrices and vectors are defined as

$$\tilde{\mathbf{A}}_i = \mathbf{V}^*\mathbf{A}_i\mathbf{V} \in \mathbb{C}^{M\times M} \quad \text{with } i = 1\ldots I, \tag{7}$$

$$\tilde{\mathbf{B}} = \mathbf{V}^*\mathbf{B} \in \mathbb{C}^{M\times T}. \tag{8}$$

4.1. Adaptivity

As demonstrated in [8], the 2-norm of the residual $\mathbf{r}_m(k_0)$ of (2) of the ROM solution $\tilde{\mathbf{x}}_m(k_0)$,

$$\mathbf{r}_m(k_0) = g(k_0)\mathbf{b}_m - \left(\sum_{i=1}^{I} f_i(k_0)\mathbf{A}_i\right)\mathbf{V}\tilde{\mathbf{x}}_m(k_0), \tag{9}$$

can be evaluated very efficiently, using reduced-order quantities only. It was suggested in [9] to employ the relative residual norm ρ,

$$\rho(k_0) = \max_{m=1\ldots T} \frac{\|\mathbf{r}_m(k_0)\|_2}{\|g(k_0)\mathbf{b}_m\|_2} \quad \text{with } m = 1\ldots T, \tag{10}$$

as an inexpensive error indicator for guiding the placement of the expansion points k_0^i: At a given stage of ROM generation, ρ is evaluated for a dense sampling $\{k_0^s\}$ of the wavenumber interval. The following expansion point is chosen where the relative residual (10) is the largest. ROM generation terminates when ρ has fallen below a user-defined threshold ρ_0 for all k_0^s.

In practice we have $M \ll N$, thus having formed the ROM, the nearfields of the antenna array are computed much more rapidly by solving (6) than the original FE system (2).

5. FARFIELD COMPUTATION

By the vector Huygens principle in the frequency domain [10], the radiation vector $\mathbf{F}$ of an arbitrary antenna array enclosed by a surface S is given by

$$\mathbf{F}(k_0, \hat{\mathbf{r}}) = \hat{\mathbf{r}} \times \oint_S e^{jk_0 \hat{\mathbf{r}}\cdot\mathbf{r}'} \mathbf{J}_s(\mathbf{r}', k_0) \, \mathrm{d}S' \times \hat{\mathbf{r}} + \frac{1}{\eta_0} \oint_S e^{jk_0 \hat{\mathbf{r}}\cdot\mathbf{r}'} \mathbf{M}_s(\mathbf{r}', k_0) \, \mathrm{d}S' \times \hat{\mathbf{r}}. \quad (11)$$

The unit vector $\hat{\mathbf{r}}$ represents the direction to the observer. The equivalent electric and magnetic surface current densities, $\mathbf{J}_s$ and $\mathbf{M}_s$, are given by

$$\mathbf{J}_s(\mathbf{r}', k_0) = \hat{\mathbf{n}}_s \times \mathbf{H}(\mathbf{r}', k_0) \quad \text{and} \quad \mathbf{M}_s(\mathbf{r}', k_0) = -\hat{\mathbf{n}}_s \times \mathbf{E}(\mathbf{r}', k_0) \quad \text{with } \mathbf{r}' \in S. \quad (12)$$

Herein, $\hat{\mathbf{n}}_s$ denotes the outward-pointing unit normal vector on the Huygens surface S. The farfields $\mathbf{E}_F$ and $\mathbf{H}_F$ are determined from (11) by

$$\mathbf{E}_F(k_0, \mathbf{r}) = -j\eta_0 k_0 \frac{e^{-jk_0 r}}{4\pi r} \mathbf{F}(k_0, \hat{\mathbf{r}}) \quad \text{and} \quad \mathbf{H}_F(k_0, \mathbf{r}) = -jk_0 \frac{e^{-jk_0 r}}{4\pi r} \hat{\mathbf{r}} \times \mathbf{F}(k_0, \hat{\mathbf{r}}). \quad (13)$$

The numerical treatment in terms of ROM quantities by means of the EIM is presented in detail in the companion paper [12].

6. NUMERICAL EXAMPLE

We consider a linear array of $T = 32$ equally spaced, perfectly conducting dipoles in the frequency range $f \in [3, 5]$ GHz. The array is suitable for arbitrary scan angles, including the endfire direction. Since analytic solutions for the element patterns are available, reference results for the ideal array, without mutual coupling, are readily constructed.

The geometry of the FE domain is shown in Fig. 1. On the outer surface absorbing boundary conditions are applied. The dipoles are excited at their centers by lumped ports of impedance $Z_P = 73\,\Omega$. We construct the ROM by the adaptive multi-point-MOR method descripted in Section 4. The FE-DD system (2) is solved by the restarted GMRES(30) iterative method with stopping criteria $\delta = 10^{-3}$; see [11]. Computational data are listed in Table 1. It can be seen that once the ROM is available, the $\mathbf{S}$ matrix (ROM evaluation for 32 RHS) at any frequency is obtained within half a second; computing the farfields at 40000 look angles takes another 13 s.

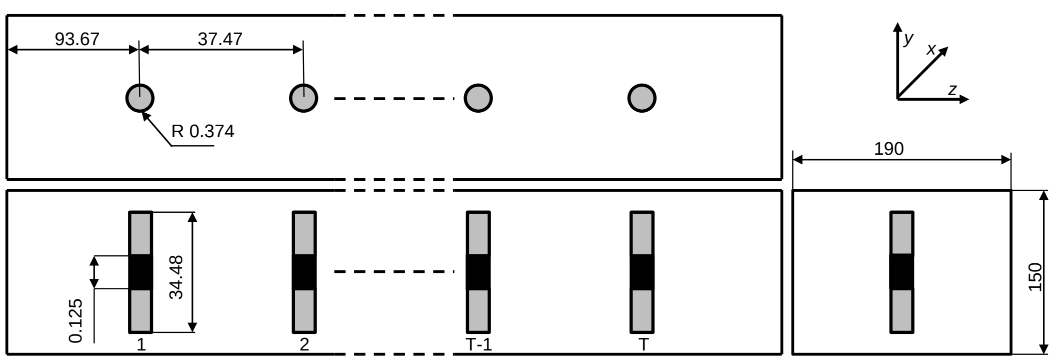

Figure 1: Linear array of dipoles. Black rectangles indicate lumped ports. Dimensions are in mm.

Table 1: Computational data*.

Model	ROM	FE-DD	Stopping criteria
Dimension	300	$4 \cdot 10^6$	-
FE-DD solution for 1 RHS (s)	-	412	-
ROM construction (h)	48	-	10^{-3}
EIM construction (h)	56	-	10^{-3}
ROM evaluation for 32 RHS (s)	$5 \cdot 10^{-1}$	-	-
Farfield evaluation at 40000 look angles (s)	13	300	-

* Matlab prototype code on Intel Core i5-4570 CPU @ 3.2 GHz.

To demonstrate the capabilities of the proposed approach, we consider three types of aperture illuminations: uniform, Dolph-Tschebycheff, and Taylor-n-bar distribution. In the latter cases, the desired side lobe level is set to be $D_s = -20$ dB. Fig. 2–Fig. 4 compare the radiation patterns of the proposed method and analytic pattern multiplication, for broadside ($\theta_s = \frac{\pi}{2}, \phi_s = 0$), intermediate ($\theta_s = \frac{\pi}{4}, \phi_s = 0$), and endfire ($\theta_s = 0, \phi_s = 0$) configurations at $f = 3.8$ GHz. Mutual coupling leads to markable differences in the side lobes and, in the endfire case, even the beamwidth of the main lobe is significantly affected. Fig. 5(a) presents the frequency response of the reflection coefficient for a central and an outer antenna element. Position-dependent detuning is clearly visible. The transmission coefficients between one radiator and its three closest neighbors are shown in Fig. 5(b). As expected, mutual coupling between immediate neighbors is strong and more pronounced at the center of the array than at its edges.

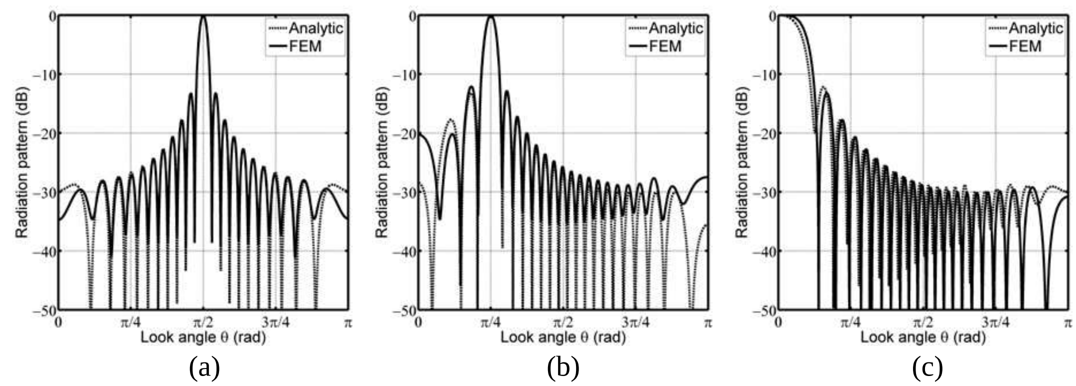

Figure 2: Uniform distribution: farfields plane $\phi = 0$ rad, $f = 3.8$ GHz. (a) Steering angle $\theta_s = \frac{\pi}{2}$ rad. (b) Steering angle $\theta_s = \frac{\pi}{4}$ rad. (c) Steering angle $\theta_s = 0$ rad.

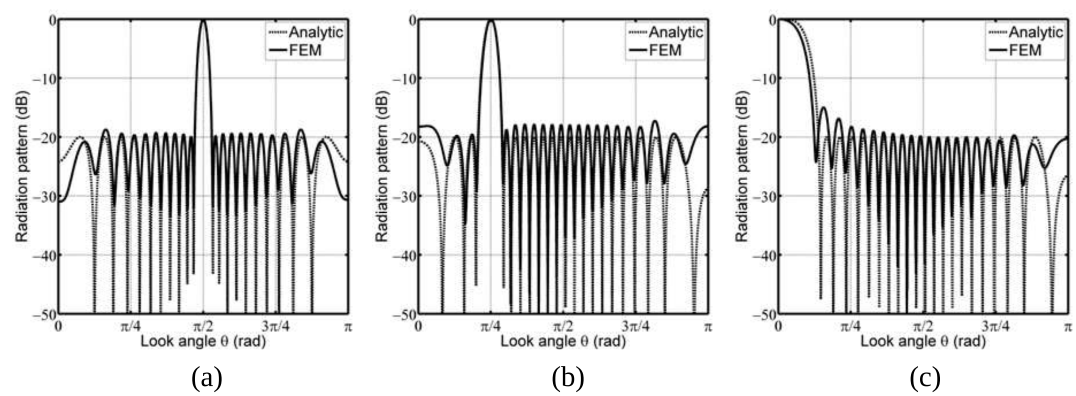

Figure 3: Dolph-Tschebycheff distribution: side lobe level $= -20$ dB, farfields plane $\phi = 0$ rad, $f = 3.8$ GHz. (a) Steering angle $\theta_s = \frac{\pi}{2}$ rad. (b) Steering angle $\theta_s = \frac{\pi}{4}$ rad. (c) Steering angle $\theta_s = 0$ rad.

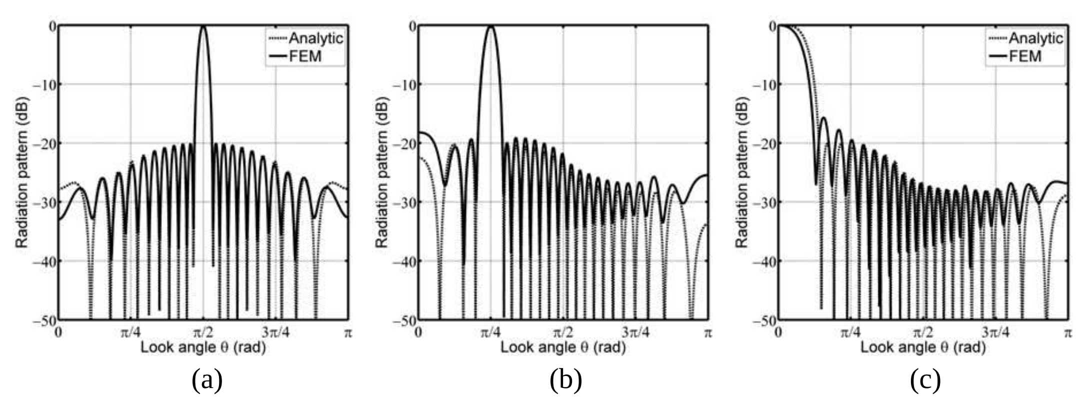

Figure 4: Taylor distribution: $n = 5$, side lobe level $= -20$ dB, farfields plane $\phi = 0$ rad, $f = 3.8$ GHz. (a) Steering angle $\theta_s = \frac{\pi}{2}$ rad. (b) Steering angle $\theta_s = \frac{\pi}{4}$ rad. (c) Steering angle $\theta_s = 0$ rad.

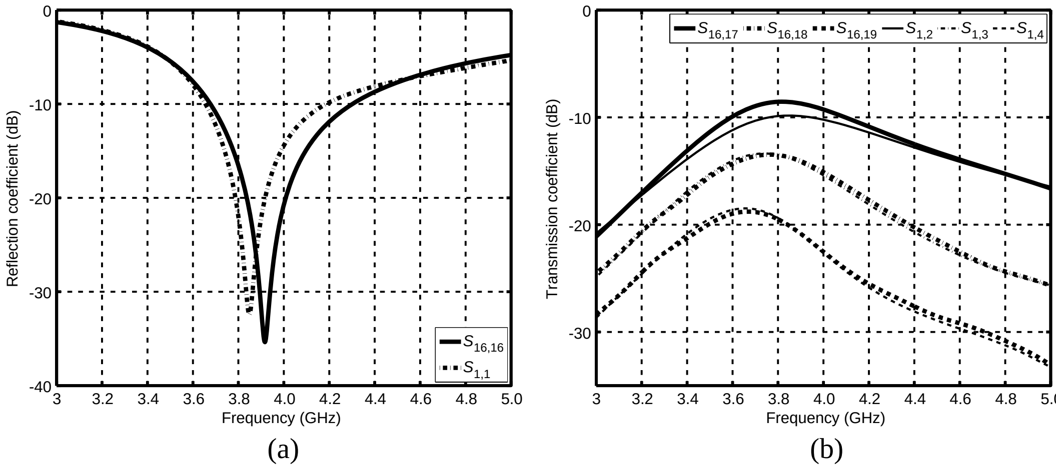

Figure 5: Frequency response of selected scattering parameters. (a) Magnitude of reflection coefficient. (b) Magnitude of transmission coefficient.

7. CONCLUSION AND OUTLOOK

A MOR-based numerical method for characterizing antenna arrays at the fields level has been proposed. It is well-suited for broad frequency bands and allows for arbitrary excitations. Numerical experiments demonstrate the accuracy and efficiency of the suggested approach. Future work will include antenna pattern synthesis, including mutual coupling of antenna elements.

REFERENCES

1. Fares, M., J. S. Hesthaven, Y. Maday, and B. Stamm, "The reduced basis method for the electric field integral equation," *J. Comput. Phys.*, Vol. 230, No. 14, 5532–5555, 2011.
2. Sommer, A., O. Farle, and R. Dyczij-Edlinger, "Efficient finite-element computation of farfields of phased arrays by order reduction," *COMPEL*, Vol. 32, No. 5, 1721–1734, 2013.
3. Rozza, G., D. B. P. Huynh, and A. T. Patera, "Reduced basis approximation and a posteriori error estimation for affinely parametrized elliptic coercive partial differential equations," *Arch. Comput. Methods Eng.*, Vol. 15, No. 3, 229–275, 2008.
4. Barrault, M., Y. Maday, N. C. Nguyen, and A. T. Patera, "An empirical interpolation method: Application to efficient reduced-basis discretization of partial differential equations," *C. R. Math. Acad. Sci. Paris*, Vol. 339, No. 9, 1721–1734, 2013.
5. Buffa, A. and P. Ciarlet, "On traces for functional spaces related to Maxwell's equations. Part I: An integration by parts formula in Lipschitz polyhedra," *Math. Meth. Appl. Sci.*, Vol. 21, 9–30, 2001.
6. Rawat, V. and J.-F. Lee, "Non-overlapping domain decomposition with second order transmission condition for time-harmonic Maxwell's equations," *SIAM J. Sci. Comput.*, Vol. 32, No. 6, 3584–3603, 2010.
7. Floch. O., A. Sommer, O. Farle, and R. Dyczij-Edlinger, "Is model-order reduction viable for the broadband finite-element analysis of electrically large antenna arrays?," Accepted for Publication in *Advances in Radio Science*.
8. Patera, A. T. and G. Rozza, "Reduced basis approximation and a posteriori error estimation for parametrized partial differential equations," *MIT Pappalardo Graduate Monographs in Mechanical Engineering*, Vol. 1, 2006–2007, 2008.
9. De la Rubia, V., U. Razafison, and Y. Maday, "Reliable fast frequency sweep for microwave devices via the reduced-basis method," *IEEE Transactions on Microwave Theory and Techniques*, Vol. 57, No. 12, 2923–2937, 2009.
10. Rothwell, E. and M. Cloud, *Electromagnetics*, 2nd Edition, CRC Press, 2008.
11. Saad, Y. and M. H. Schultz, "GMRES: A generalized minimal residual algorithm for solving nonsymmetric linear systems," *SIAM J. Sci. Stat. Comput.*, Vol. 7, No. 3, 856–869, 1986.
12. Sommer, A., O. Floch, O. Farle, and R. Dyczij-Edlinger, "Parametric near-field-to-far-field transformation by precomputed empirical-interpolation patches," to Appear in *PIERS Proceedings*, 2015.